OBSERVATIONS OF CENTRAL TOROIDAL ROTATION IN ICRF HEATED ALCATOR C-MOD PLASMAS

J.E. RICE, M. GREENWALD, I.H. HUTCHINSON, E.S. MARMAR,
Y. TAKASE, S.M. WOLFE, F. BOMBARDA*
Plasma Science and Fusion Center,
Massachusetts Institute of Technology,
Cambridge, Massachusetts,
United States of America

* Associazione ENEA–Euratom per la Fusione,
Frascati, Rome,
Italy

ABSTRACT. Impurity toroidal rotation has been observed in the centre of Alcator C-Mod ion cyclotron range of frequencies (ICRF) heated plasmas, from the Doppler shifts of argon X ray lines. Rotation velocities greater than 1.2×10^7 cm/s ($\omega = 200$ krad/s) in the co-current direction have been observed in H mode discharges that had no direct momentum input. There is a correlation between the increase in the central impurity rotation velocity and the increase in the plasma stored energy (confinement enhancement), induced by ICRF heating, although other factors may be at play. The toroidal rotation velocity is highest near the magnetic axis, and decreases with increasing minor radius. A radial electric field of 300 V/cm at $r/a = 0.3$ has been inferred from the force balance equation. The direction of the rotation changes when the plasma current direction is reversed, remaining co-current. Impurity toroidal rotation in ICRF heated plasmas is in the direction opposite to the rotation in ohmic L mode plasmas; co-current rotation has also been observed during purely ohmic H modes. When the ICRF heating is turned off, the toroidal rotation decays with a characteristic time of order 50 ms, similar to the energy confinement time, and much shorter than the calculated neoclassical momentum damping time.

1. INTRODUCTION

Rotation plays an important role in the transition from L to H mode [1–4]. Poloidal rotation in the edge plasma region has been closely associated with the L–H transition [5–7], and toroidal momentum confinement is well correlated with energy confinement [8–11]. While there have been several diagnostic systems designed to measure impurity toroidal rotation in tokamak plasmas [8–33], most of the observations have been made in plasmas with an external momentum source, usually provided by neutral beams. Toroidal impurity rotation in ohmic plasmas (no net momentum input) is consistent with neoclassical predictions [24, 33, 34]; in ohmic L mode discharges, impurities rotate in the direction opposite to the plasma current, so in general the assumption that the majority ions and impurities (which are most often measured) rotate in the same way might be questionable [34]. In neutral beam heated plasmas, which have substantial direct momentum input, the toroidal momentum confinement time is much shorter than the neoclassical predictions [8–11]. Toroidal rotation profiles have been used to infer E_r [8, 11]. In some neutral beam plasmas with ion cyclotron range of frequencies (ICRF) heating, the rotation has been seen to drop significantly during the RF pulse [21]. Countercurrent toroidal rotation associated with ion orbit loss in neutral beam and ICRF heated plasmas has been observed [26, 31], and the effects of electron loss in LHCD plasmas have been seen [29]. It is difficult to separate the contribution to the rotation from the direct momentum input of the neutral beams and the rotation that may be associated with (or induced by) H modes, although some information has been gleaned from balanced or perpendicular beam injection [8, 11]. ICRF-only heated discharges provide an opportunity for the study of toroidal rotation in plasmas with no direct momentum input. Co-current rotation in ICRF-only plasmas [27, 32] has been documented, alternately explained by high energy ion loss [27] and the effects of the ion pressure gradient [32], and the role of neutrals in slowing down toroidal rotation has been noted [32].

In this article, the results of impurity toroidal rotation measurements in ICRF heated Alcator C-Mod

[35] plasmas are presented. The experimental set-up is described, and the magnitude and direction of the rotation are documented. Rotation time histories in a variety of different plasmas are presented, and the correlation between the velocity (momentum) increase and the plasma stored energy increase (confinement improvement) is demonstrated. Radial profiles of the rotation velocity are presented with the inferred E_r, and the decay in the velocity after the ICRF power is turned off is shown.

2. EXPERIMENT DESCRIPTION

The observations presented here were obtained from the Alcator C-Mod [35] tokamak, a compact (major radius (R) of 67 cm, typical minor radius of 22 cm and $\kappa \leq 1.8$), high field device ($2.6 \leq B_{\mathrm{T}} \leq 7.9$ T), which has operated with plasma currents between 0.23 and 1.5 MA and average electron densities between 0.24 and 4.4×10^{20} m^{-3}. Up to 3.5 MW of ICRF power at 80 MHz [36] are available, from two dipole antennas, each with 0π phasing; the cases described here are all with H minority heating. During most of the operation, the plasma current is in the clockwise direction as viewed from the top of the machine. X ray spectra were recorded with a spatially fixed von Hamos type crystal X ray spectrometer [37], whose line of sight is tangential to the plasma axis, pointing in the counterclockwise direction, as seen from above, and a vertically scannable von Hamos type X ray spectrometer array [38]. The array consists of five spectrometers, two of which are scannable in a vertical plane oriented 6° off a major radius, directed at the plasma axis, in a slight counterclockwise view. The other three spectrometers have a similar slight (6°) clockwise view. The spectrometer layout with respect to Alcator C-Mod is shown in Fig. 1. All spectrometers have a spatial resolution of 2 cm. Rotation velocities have been determined

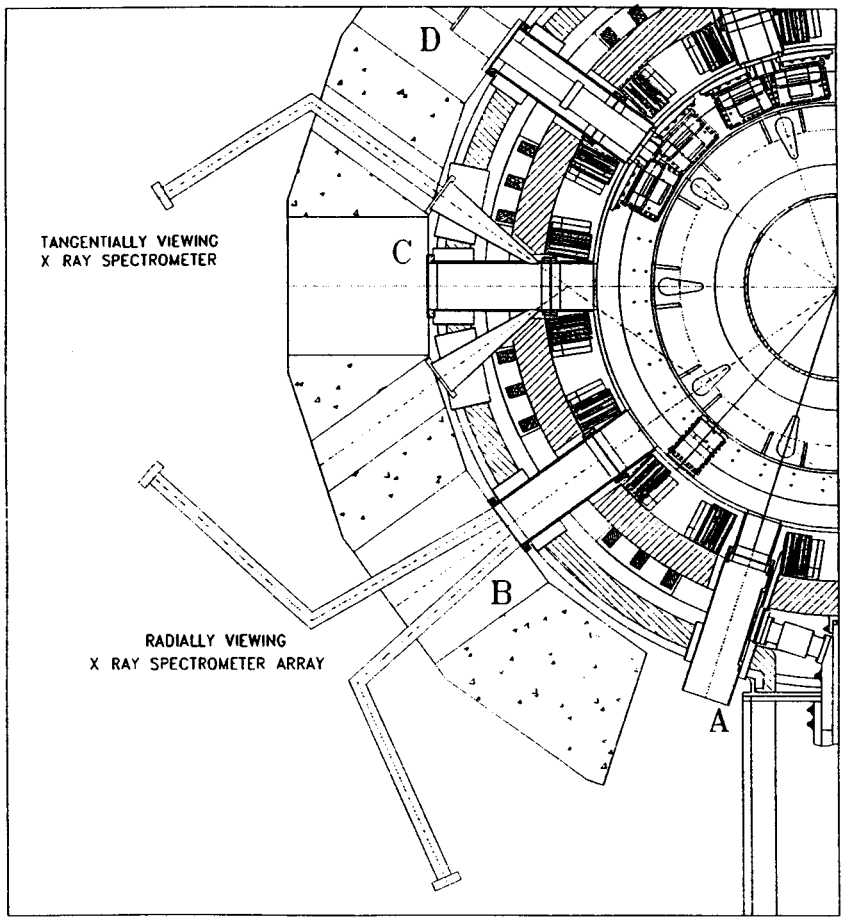

FIG. 1. Experimental layout. The magnetic axis is shown by the circular chain curve.

from the Doppler shifts of the Ar^{17+} Lyman α doublet [39, 40] (1s $^1S_{1/2}$–2p $^2P_{3/2}$ at 3731.12 mÅ, and 1s $^1S_{1/2}$–2p $^2P_{1/2}$ at 3736.53 mÅ) and the Ar^{16+} forbidden line, z [41, 42] (1s2p $^3S_1$–1s^2 $^1S_0$ at 3994.28 mÅ). The forbidden line in the helium-like argon spectrum is utilized for the Doppler shift measurement instead of the (usually) brighter resonance line because there is no contamination from nearby unresolved high-n satellites, which can give rise to an apparent shift due to changes in relative intensity [19]. This is not a problem for the Lyman α doublet, since its high-n satellites have been measured to be negligibly weak. Spectra are typically collected every 20 to 50 ms during plasma discharges. Argon is routinely injected into Alcator C-Mod plasmas through a piezoelectric valve, to provide X ray transitions for Doppler width ion temperature measurements [43]. Absolute wavelength calibration for the tangentially viewing spectrometer was obtained from the potassium K_α lines generated from a KCl fluorescence X ray source [40]. There was no wavelength calibration for the spectrometer array viewing at $\pm 6°$, so for those measurements all velocities are relative to the pre-RF conditions.

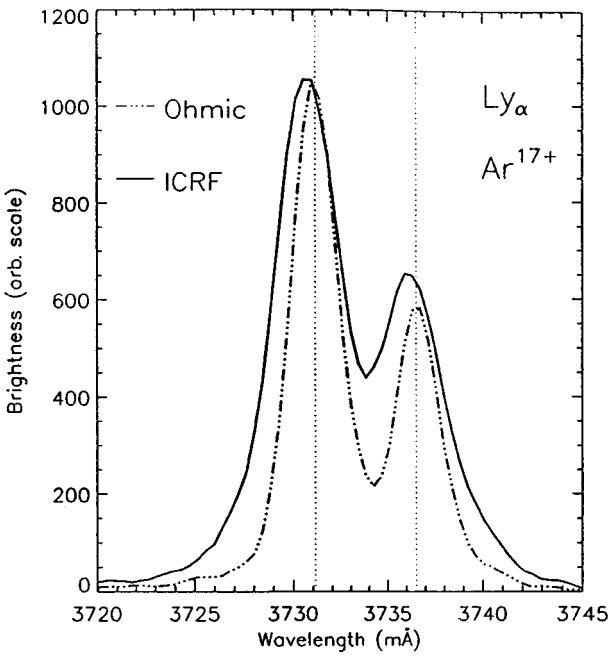

FIG. 2. X ray spectra of the Ar^{17+} Lyman α doublet for the ohmic (chain curve) and ICRF (solid curve) portions of a 0.8 MA clockwise current discharge with 2 MW of ICRF power. The Lyman α at-rest wavelengths are shown by the thin vertical lines.

3. OBSERVATIONS OF TOROIDAL ROTATION AND SCALINGS

Shown in Fig. 2 are X ray spectra including the hydrogen-like argon doublet employed for the rotation analysis, obtained using the tangentially viewing spectrometer from a 0.8 MA discharge with the current in the clockwise direction. The thin vertical lines indicate the at-rest wavelengths. The spectrum shown by the chain curve is from the ohmic portion; during the steady state period of ohmic L mode discharges, the rotation velocities are typically small (in the countercurrent direction) and there is little shift [33]. Shown by the solid curve in the figure is a spectrum taken during the H mode phase of the same discharge, induced by 2 MW of ICRF power. The two spectra have been normalized in intensity to emphasize the wavelength shift. Since the spectrometer was viewing tangentially counterclockwise, and the solid spectrum is blue shifted, the argon is rotating clockwise, in the same direction as the plasma current during the RF pulse. This is in the direction opposite to the rotation of impurities in ohmic L mode plasmas [8, 24, 33, 4]. The magnitude of the shift is $\sim$0.5 mÅ, which yields a toroidal rotation velocity of (0.5 mÅ/3731.1 mÅ) $\times\, c = 4.0 \times 10^6$ cm/s, in the co-current direction. Since the major radius of Alcator C-Mod is 67 cm, this corresponds to an angular rotation speed of 60 krad/s.

The toroidal rotation may also be determined from the helium-like argon forbidden line. Shown in Figs 3(a) and (b) are spectra recorded from a spectrometer viewing the plasma midplane, at an angle of 6° from a major radius, in a slight counterclockwise view. The spectra of Fig. 3(a) were obtained from a 1.1 MA discharge (clockwise current), and there is a blue shift of 0.13 ± 0.01 mÅ during the H mode phase (spectrum shown by the solid curve), when the plasma stored energy increased by 0.12 MJ. This corresponds to a toroidal rotation velocity increase of (0.13 mÅ/3994.3 mÅ)/sin(6°) $\times\, c = 1.0 \times 10^7$ cm/s (150 krad/s), in the co-current direction. The spectra of Fig. 3(b) were obtained with the same view from a 1.0 MA discharge with the plasma current in the counterclockwise direction, and there is a red shift of 0.07 ± 0.01 mÅ during the 2.7 MW ICRF pulse, indicating that the argon is rotating in the counterclockwise direction, again co-current. This L mode discharge had a stored energy increase of 45 kJ, when the magnitude of the toroidal rotation velocity increased by 5.3×10^6 cm/s, and still opposite to the rotation direction in ohmic discharges. The phasing of

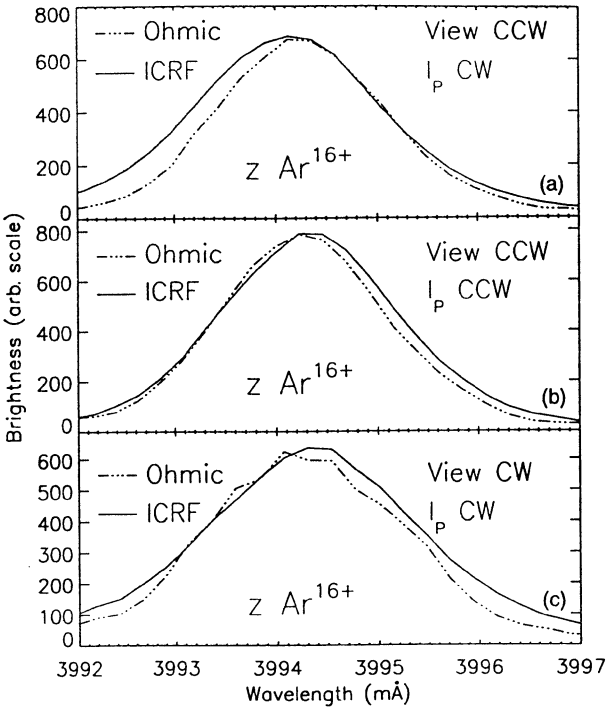

FIG. 3. X ray spectra of the Ar^{16+} forbidden line for the ohmic (chain curve) and ICRF (solid curve) portions of: (a) a 1.1 MA clockwise current discharge with 2 MW of ICRF power and 6° counterclockwise view, (b) a 1.0 MA counterclockwise current discharge with 2.7 MW of ICRF power and 6° counterclockwise view, (c) a 0.8 MA clockwise current discharge with 2.7 MW of ICRF power and 6° clockwise view.

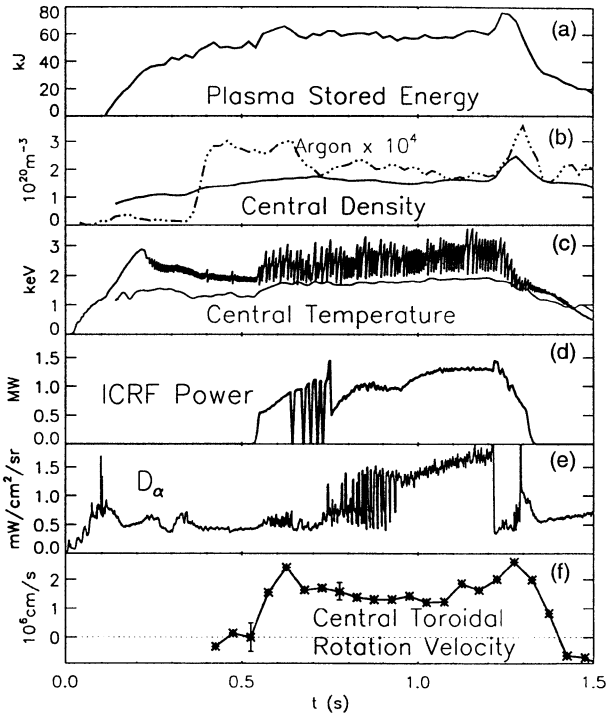

FIG. 4. Time histories of several parameters for a 5.4 T, deuterium L mode discharge: (a) plasma stored energy, (b) central electron density (solid curve) and central argon density (chain curve, $\times 10^4$), (c) central electron temperature (curve showing sawteeth) and central ion temperature (smooth curve), (d) ICRF power, (e) D_α emission. In (f) the central toroidal rotation velocity of argon ions is shown, with typical error bars being given.

the RF antennas for this case was the same as that in Fig. 3(a). Shown in Fig. 3(c) are spectra recorded from a 6° clockwise view from a 0.8 MA discharge with the plasma current in the clockwise direction, and there is a red shift of 0.08 ± 0.01 mÅ during the 2.7 MW ICRF pulse, indicating that the argon is rotating at 6.0×10^6 cm/s, in the co-current clockwise direction. The line of sight of the spectrometer used for this measurement was also pointing 8 cm below the plasma midplane for this discharge, and could therefore be sensitive to a poloidal component of the rotation. However, for this same discharge, the spectrometer with a 6° counterclockwise toroidal view was also pointing 8 cm below the midplane and recorded an equal and opposite line shift, indicating that any poloidal component to the rotation velocity is $\leq 3 \times 10^5$ cm/s (the detection limit) at this radius. The widths of the lines in the ICRF spectra (those shown by solid curves) are broader, owing to a simultaneous increase in the ion temperature, and the intensities of the lines in the ohmic and ICRF cases have been normalized in order to emphasize the wavelength shift.

The time histories of several parameters of interest for a 5.4 T, 0.82 MA deuterium L mode plasma are shown in Fig. 4. Argon is injected in a 50 ms wide pulse at 0.3 s into the discharge, and the subsequent central argon density ($\times 10^4$), along with the central electron density, is shown in Fig. 4(b). The impurity content α, defined as $n_I Z_I^2 / n_i Z_i^2$ (where I denotes impurity and i denotes majority ion), is everywhere less than 0.06 for this discharge. The RF is turned on at 0.54 s (Fig. 4(d)), and there is a subsequent increase in the electron and ion temperatures (Fig. 4(c)) and a very modest increase in the stored energy (Fig. 4(a)). This L mode plasma also begins to rotate in the co-current direction at about 1.5×10^6 cm/s, as shown in Fig. 4(f). This plasma briefly enters H mode after 1.2 s, as evident in the drop of the D_α signal (Fig. 4(e)), and increases in the stored energy and the electron and argon densities. There is also a slight increase in the rotation

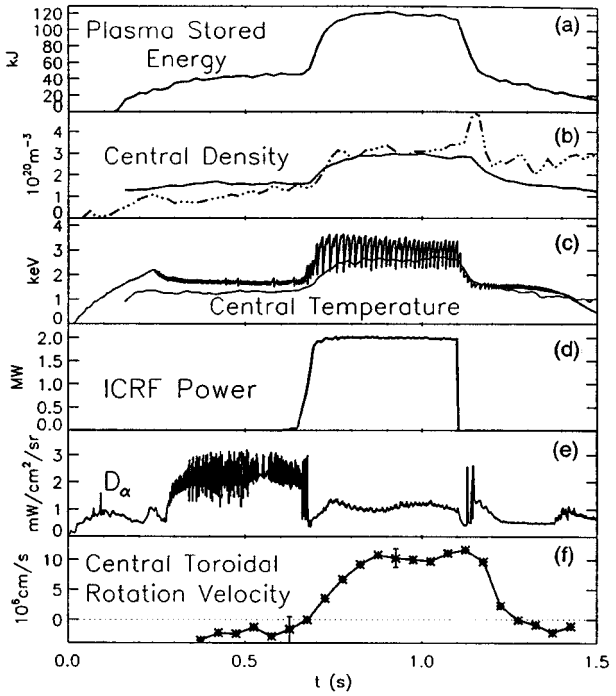

FIG. 5. Time histories of several parameters for a 5.3 T, deuterium H mode discharge. The legend is the same as that in Fig. 4.

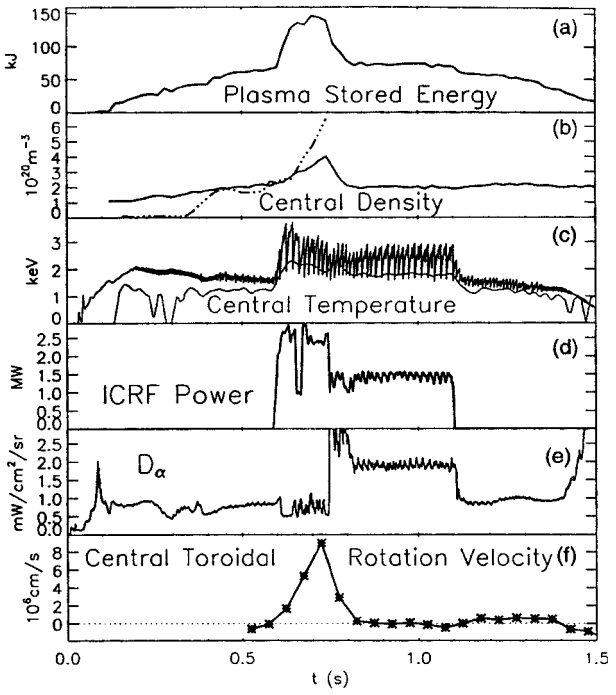

FIG. 6. Time histories of several parameters for a 5.4 T, deuterium H mode discharge. The legend is the same as that in Fig. 4.

velocity. The time histories of these same parameters for a 5.3 T, 0.82 MA deuterium H mode plasma are shown in Fig. 5. In this case, there is a dramatic increase in the stored energy of 75 kJ when the plasma enters H mode (∼0.68 s), and the central rotation velocity reaches over 1.0×10^7 cm/s. An estimate of the rotation contribution to the total stored energy is about 10 kJ. The central rotation velocity increases over a time period of 100 ms or so after the H mode begins, indicating that the central toroidal rotation is a consequence of the H mode transition. There are also substantial increases in the electron and argon densities, and in the electron and ion temperatures during the same time. Another H mode discharge is shown in Fig. 6; in this case the plasma enters H mode at 0.6 s when the D_α drops, and the stored energy, rotation velocity and densities and temperatures all increase. This plasma returns to L mode at 0.75 s (when the RF power decreases by a factor of 2). The stored energy, electron density and rotation velocity all then approach their previous L mode values, while the electron and ion temperatures remain elevated. This suggests a correlation between the rotation velocity increase and the stored energy increase, and not just in the ion temperature or gradient. However, the D_α emission level greatly increases after 0.8 s, suggesting an increased edge neutral density slowing down the rotation.

The correlation between the plasma rotation and energy is demonstrated in Fig. 7; there is a general increase in the impurity toroidal rotation velocity increase during the ICRF pulse and the stored energy increase, over nearly 2 orders of magnitude, although stored energy increases less than 5 kJ are difficult to measure. This data set includes a range of RF powers between 0.5 and 3.1 MW, central electron densities between 0.9 and 5.9×10^{20} m^{-3}, plasma currents between 0.6 and 1.2 MA and clockwise and reverse currents, in both L and H mode plasmas, with H factors between 0.75 and 2.3. The points shown as asterisks (diamonds) are from H mode (L mode) plasmas and the four points shown as 'plus signs' are from purely ohmic H mode discharges, which also rotate in the co-current direction after the plasma undergoes the L–H transition. For the ICRF heated L and H mode discharges, the stored energy increase induced by the RF is used, while for the ohmic points, the stored energy increase due to the onset of the H mode is considered. The points shown as triangles are from reversed current discharges (rotating in the opposite direction to the other points in the figure, but still co-current), which had substantial stored

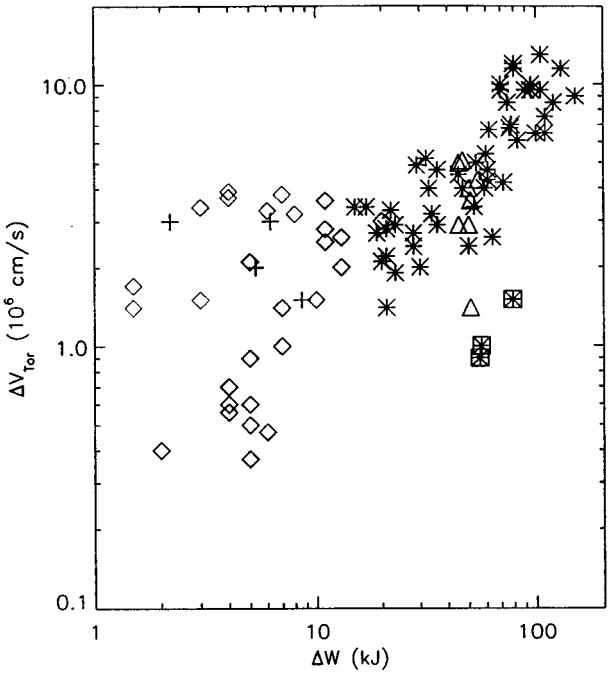

FIG. 7. Toroidal rotation velocity increase during the ICRF pulse as a function of the plasma stored energy increase in H mode (L mode) discharges shown as asterisks (diamonds). The points shown as triangles are from plasmas with reversed current. The points shown as asterisks surrounded by boxes are from high-D_α H mode discharges, those shown as light diamonds are from shots with falling argon density and those shown as plus signs are from ohmic H mode discharges.

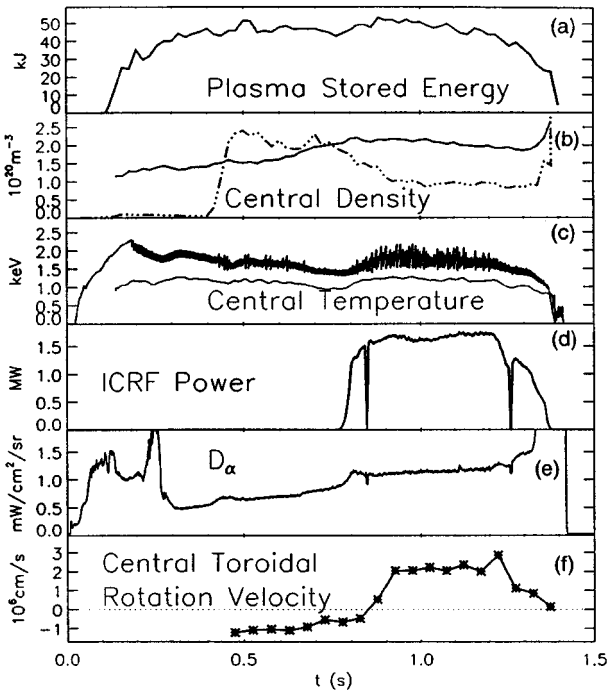

FIG. 8. Time histories of several parameters for a 5.4 T, deuterium L mode discharge. The legend is the same as that in Fig. 4.

energy and rotation velocity increases, but were not strict H mode plasmas because of the absence of any drop in D_α emission. While there is a distinct correlation, especially for large stored energy increases, some of the points are somewhat far from the main trend. The three points surrounded by boxes are from H mode discharges that had high levels of D_α radiation (enhanced D_α discharges [44, 45]), and do not rotate as fast as otherwise similar discharges, an effect that has also been observed in JET [32] plasmas. The points shown as thin diamonds, which seem to be rotating rather quickly for such a small stored energy increase, are from one particular L mode run that had a peculiar argon density time history. One of these discharges is shown in Fig. 8; in this case the argon density, which is around 2×10^{16} m^{-3} before the ICRF pulse, drops over a factor of 2 when the RF is turned on, and the plasma begins rotating in the co-current direction at 2×10^6 cm/s. At this time there is also an increase in the electron density, and in the electron and ion temperatures, but only a slight increase in the stored energy. Although the argon ions are rotating relatively quickly for this modest stored energy increase, there are fewer of them so the total argon momentum increase is not so large. This suggests that perhaps a quantity of interest for comparison with the stored energy increase is the increase in the argon momentum or angular momentum density. The quantity $\Delta(n_{\rm Ar}V_{\rm Tor})$, which is proportional to both the argon momentum density ($n_{\rm Ar}m_{\rm Ar}V_{\rm Tor}$) and the argon angular momentum density ($n_{\rm Ar}m_{\rm Ar}V_{\rm Tor}R$), is plotted as a function of the stored energy increase in Fig. 9. The main difference between this figure and Fig. 7 is that the points from the falling argon density run (cf. Fig. 8) are now closer to the main group of points. (The four ohmic H mode points from Fig. 7 have not been included in Fig. 9 because the argon density was not measured for these discharges.) However, small increases in the stored energy are hard to measure and less interesting, and it is not implied that the argon momentum is an important player in the overall momentum balance. The overall scatter in the points has increased slightly, but the trend for the highest rotation points persists. Attempts to find a correlation between the rotation velocity increase and other parameters such as the RF power, ion temperature or ion pressure increase have resulted in very

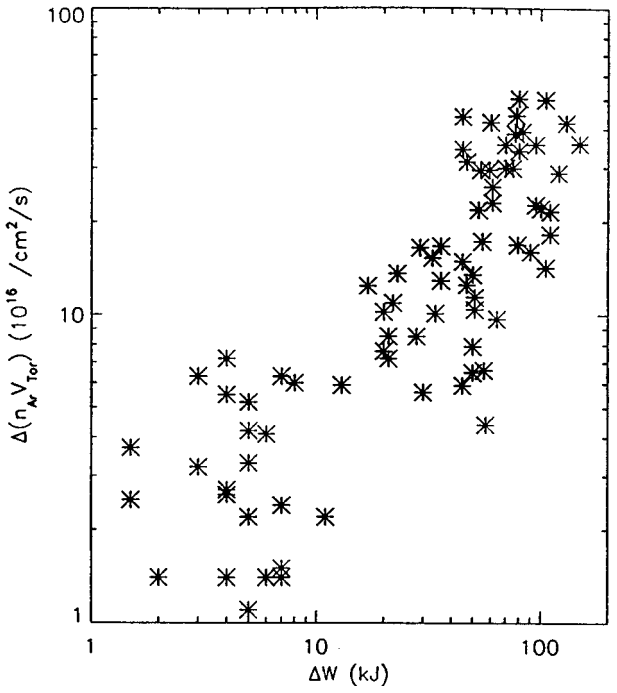

FIG. 9. Increase in the product $n_{\mathrm{Ar}}V_{\mathrm{Tor}}$ (proportional to the argon (angular) momentum density increase) as a function of plasma stored energy increase.

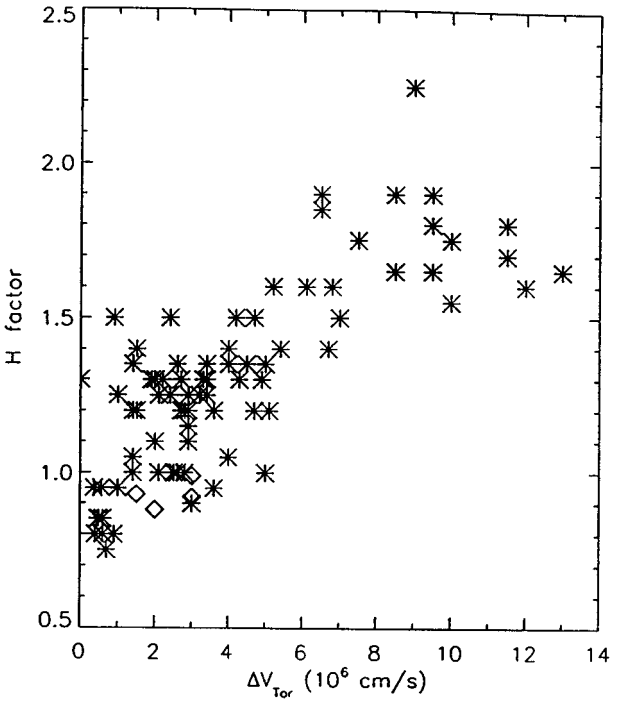

FIG. 10. H factor as a function of toroidal rotation velocity increase. The points shown as diamonds are from ohmic H mode discharges.

large scatter in the data points, with no suggestive trends resulting. The fact remains that the plasmas with the highest rotation velocities generally have the best energy confinement. This is emphasized in Fig. 10, where the ITER-89P H factor [46] is plotted as a function of rotation velocity increase, for all of the points of Fig. 7. The plasmas that rotate the fastest have the highest H factors. There is a continuous range of L and H mode behaviour presented here; some of the high H factor L mode plasmas rotate more quickly than the lower H factor H mode plasmas, and there is no sharp dichotomy. The purely ohmic H mode points, from rather unspectacular 0.6 MA, 3.4 T discharges, are shown by the diamonds.

4. ROTATION VELOCITY PROFILES AND E_r

Some radial profile information on the rotation velocity is available from vertical scans of the spectrometer array. Two of the spectrometers were scanned on a shot-to-shot basis during three very similar 5.4 T, 0.8 MA deuterium H mode discharges, which had stored energy increases of 75 kJ during the 2.0 MW ICRF pulses. Shown in Fig. 11 is the radial profile of the toroidal rotation velocity; the velocity is highest in the plasma centre, and rapidly falls off with minor radius. For these plasmas, the last closed flux surface on the midplane was at 20.5 cm. The points shown as asterisks are from the spectrometer with a 6° counterclockwise view, and the spectral lines were blue shifted in this case; the points shown as boxes are from the spectrometer with a 6° clockwise view, and the lines were red shifted (Fig. 3). For the two points near 5.5 cm, both spectrometers were viewing at nearly the same *poloidal* angle. Since the wavelength shift was equal in magnitude at this radius, but opposite in sign, and the two spectrometers had opposite *toroidal* views, the rotation at this radius must mostly be toroidal, with an upper limit for the poloidal component $\leq 3 \times 10^5$ cm/s. For the point at 9.1 cm, the signal level before the H mode was very low, and there is a large error in the pre-RF rotation velocity (as in Fig. 3(c)). At this radius, in this case, it is not possible to make a statement about any poloidal component in the velocity. The rotation velocity decrease with radius has been seen in many neutral beam heated plasmas [8, 9, 11, 23, 30], and has been predicted from theory for TFTR plasmas ('self-generated' rotation) [3].

An independent measurement of central plasma rotation has been obtained from the frequency of the

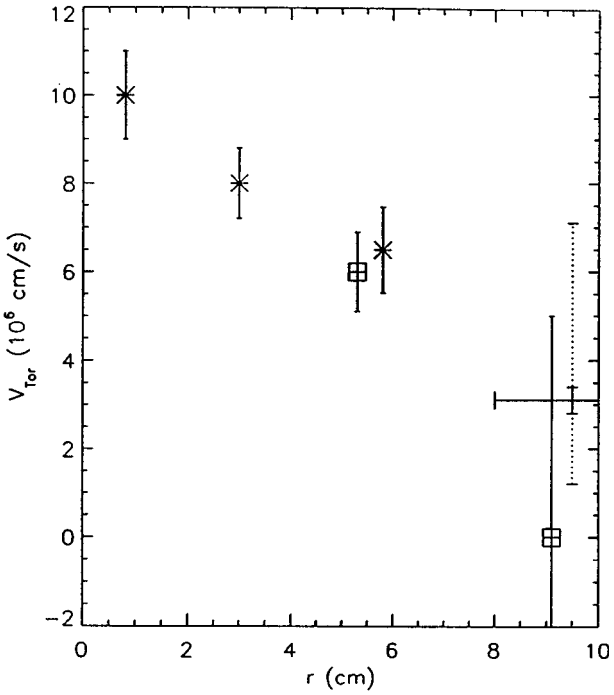

FIG. 11. Toroidal rotation velocity as a function of radius for three identical H mode discharges. The points shown by asterisks are from a counterclockwise view; the points shown by boxes are from a clockwise view. The point at 9.5 cm is the sawtooth precursor rotation velocity.

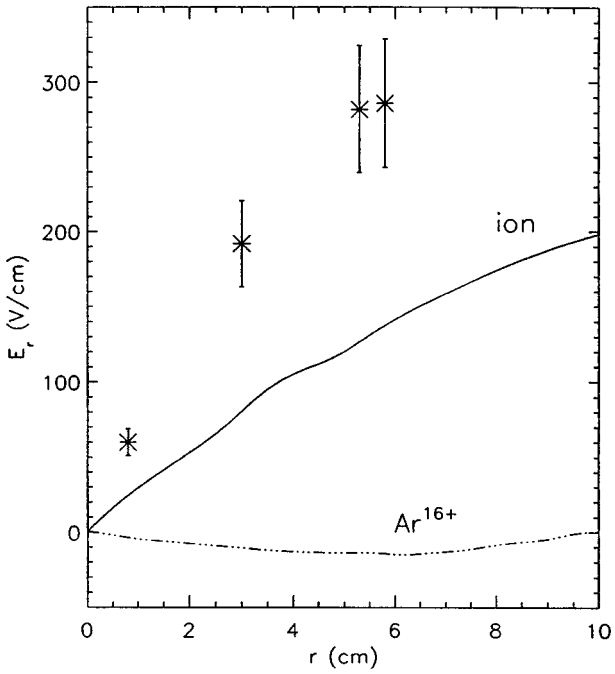

FIG. 12. Inferred E_r, from the observed argon toroidal rotation velocity profile and the computed poloidal magnetic field, as a function of minor radius. Shown by the smooth curve is the negative of the ion (deuteron) diamagnetic term calculated from the measured ion pressure gradient, and shown by the chain curve is the negative of the Ar^{16+} diamagnetic term.

sawtooth precursors, which are large during H mode, and can be observed both with the fast ECE temperature measurements and via magnetic perturbation (Mirnov) coils outside the plasma. From the frequency of these $n = 1$ modes an equivalent velocity is deduced, which is taken to be toroidal although the measurement itself cannot distinguish between toroidal and poloidal rotation. Typically, the velocity rises rapidly from a low value before the plasma enters H mode and peaks about 0.1 s later, settling thereafter to a steady state level about 10 to 20% less than its peak. It has the co-current direction, the same as that of the argon. The point at 9.5 cm in Fig. 11, shown as a solid vertical error bar, indicates the range of observed mode velocities for the shots in this series. The associated horizontal error bar indicates the range of uncertainty of the midplane sawtooth inversion radius deduced from the electron cyclotron emission (ECE).

The theoretical rotation velocity [47] of the sawtooth precursor relative to the frame in which $E_r = 0$ may be between the electron diamagnetic velocity if the mode is resistive, and half the ion diamagnetic velocity if the mode is ideal. One may then deduce a velocity of the argon ions, which are essentially at rest in the $E_r = 0$ frame, as will be demonstrated below. The argon velocity deduced depends on what is assumed about this theoretical relative velocity. The dotted error bar in Fig. 11 shows the range of the corresponding argon velocities obtained from the extremes of the relative mode rotation assumption.

An estimate of the contribution to E_r from the toroidal rotation, or the required E_r needed to give rise to the toroidal rotation, can be made from the force balance equation

$$E_r = \nabla P/neZ + V_{\mathrm{Tor}} B_{\mathrm{P}} - V_{\mathrm{Pol}} B_{\mathrm{T}}. \qquad (1)$$

The quantity $V_{\mathrm{Tor}} B_{\mathrm{P}}$ for argon as a function of minor radius is shown in Fig. 12 for the rotation profile of Fig. 11, where the poloidal magnetic field has been computed from the EFIT code [48]. The equivalent E_r is nearly 300 V/cm at $r/a = 0.3$. For comparison, the negative of the ion diamagnetic term, $-\nabla P_{\mathrm{i}}/(en_{\mathrm{i}})$, is also shown, calculated from the measured ion temperature profile and the computed ion density profile, and is everywhere a factor of 2 smaller. The Ar^{16+} diamagnetic contribution,

$\nabla P_{Ar^{16+}}/(16en_{Ar^{16+}})$, calculated from the measured ion temperature profile and the measured Ar^{16+} density profile (also shown as being negative in the figure) is negligible and the argon poloidal rotation term has been ignored inside $r/a = 0.3$. Similar E_r profiles have been deduced in PBX-M neutral beam heated discharges [11], and directly measured in ISX-B plasmas [49]. Using the upper limit for the measured poloidal rotation at $r/a = 0.3$ and the measured toroidal magnetic field could give rise to a substantial fraction of the contribution of the toroidal velocity term in Eq. (1). However, since no poloidal velocity was actually measured, and since the sign of the contribution is then unknown, Fig. 12 must be taken with the caveat of ignoring the poloidal rotation term. From Eq. (1) the ion (deuteron) rotation velocity can be estimated; the electric field has been determined from the argon toroidal rotation (Fig. 12). Ignoring ion poloidal rotation near the centre, the ion toroidal rotation velocity is larger by the ion diamagnetic term, and so the ions rotate about 50% faster than the argon ions, inside $r/a = 0.3$. If the ions rotate at 1.5×10^7 cm/s, then they carry 700 A/cm^2, about half the central current density. Conversely, the electrons rotate about 50% slower than the argon, because of the negative charge in the diamagnetic term.

Since there is negligible momentum input from ICRF waves launched with 0π phasing and therefore the input torque is unknown, it is not possible to calculate the momentum confinement time directly during the ICRF pulse. From the decay in the rotation velocity after the ICRF heating is turned off, an estimate for the central momentum confinement may be derived. The time history of the rotation velocity near the end of the ICRF heating pulse is shown in Fig. 13; the toroidal rotation decays with a 1/e time of 68 ms, a value close to the energy confinement time of 52 ms. This is much faster than the 3 s predicted for the neoclassical toroidal rotation damping time from Eq. (36) in Ref. [50]. The observed decay time and the spin-up time at the beginning of the ICRF heating pulse are similar (and similar to the rise and decay of the stored energy, Fig. 5).

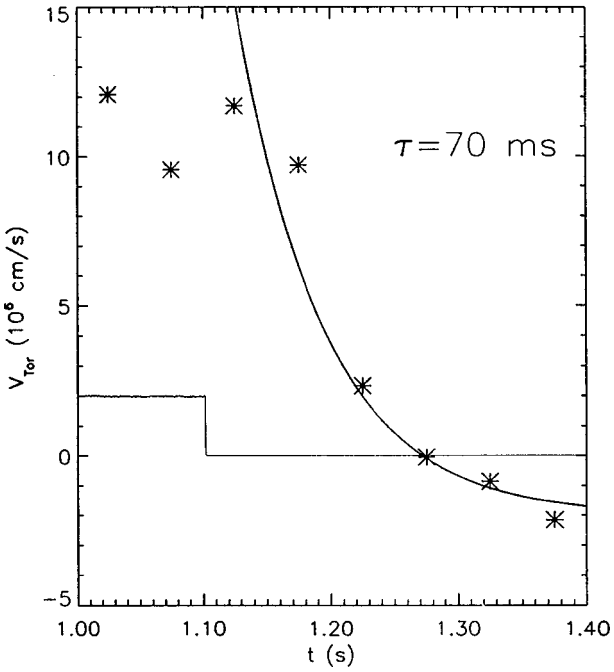

FIG. 13. Decay of the toroidal rotation velocity after the ICRF pulse is turned off, for an H mode discharge. The solid curve is the best fit exponential decay, and the RF pulse, which peaks at 2 MW, is shown by the thin line.

5. CONCLUSIONS

The central impurity toroidal rotation has been measured from the Doppler shift of X ray lines from argon in Alcator C-Mod ICRF heated plasmas. During the ICRF pulse, and in the absence of direct momentum input, the rotation is in the co-current direction (opposite to that during the ohmic portion). The mechanism for this rotation remains obscure although radial electric fields generated by strong non-ambipolar diffusion may be present. When the plasma current direction is reversed, the rotation during ICRF heating also switches, maintaining the co-current direction. The magnitude of the rotation is largest ($\sim 1.3 \times 10^7$ cm/s, 200 krad/s) during the best H mode discharges. The magnitude of the rotation velocity during ICRF heating increases with the stored energy increase, regardless of input power or electron density, over a range of 2 orders of magnitude. Some of the L mode discharges with the lowest stored energy increase had relatively high argon rotation velocities, but accompanied by a substantial decrease in the argon density, suggesting a possible correlation between the plasma stored energy increase and the argon (angular) momentum density increase. There are also some discharges, which had a large stored energy increase with very modest rotation velocity increase, that also had greater D_α emission during the H mode phase, suggesting that a higher edge neutral density may hinder the rotation. Certainly the plasmas with the highest

H factors rotate the fastest. In general, the rotation is not an effect only of H mode per se; some high H factor L mode plasmas rotate faster than some modest H factor H mode plasmas. Co-current rotation has also been observed during purely ohmic H modes. The toroidal rotation velocity is peaked at the magnetic axis, and falls off quickly with minor radius. There is no evidence for a poloidal component of the rotation velocity inside of 6 cm. Values of E_r up to 300 V/cm at $r/a = 0.3$ have been inferred. The rotation velocity decays with a characteristic time between 50 and 100 ms after the ICRF is turned off, comparable to the energy confinement time, and much shorter than the predicted neoclassical momentum slowing down time.

ACKNOWLEDGEMENTS

The authors would like to thank K. Burrell, P. Diamond, S. Migliuolo and J. Goetz for helpful discussions, J. Terry for D_α measurements, J. Irby for electron density measurements, A. Hubbard and P. O'Shea for electron temperature measurements, C. Fiore for ion temperature measurements, Y. Wang for argon density profiles and the Alcator C-Mod operations and RF groups for expert running of the tokamak. This work has been supported at MIT by USDOE Contract No. DE-AC02-78ET51013.

REFERENCES

[1] SHAING, K.C., CRUME, E.C., Phys. Rev. Lett. **63** (1989) 2369.
[2] BURRELL, K.H., et al., in Plasma Physics and Controlled Nuclear Fusion Research 1994 (Proc. 15th Int. Conf. Seville, 1994), Vol. 1, IAEA, Vienna (1996) 221.
[3] DIAMOND, P.H., et al., ibid., Vol. 3, p. 323.
[4] MOYER, R.A., et al., Phys. Plasmas **2** (1995) 2397.
[5] GROEBNER, R.J., et al., Phys. Rev. Lett. **64** (1990) 3015.
[6] WAGNER, F., et al., in Plasma Physics and Controlled Nuclear Fusion Research 1990 (Proc. 13th Int. Conf. Washington, DC, 1990), Vol. 1, IAEA, Vienna (1991) 277.
[7] MIURA, Y., et al., ibid., p. 325.
[8] SUCKEWER, S., et al., Nucl. Fusion **21** (1981) 1301.
[9] BURRELL, K.H., et al., Nucl. Fusion **28** (1988) 3.
[10] KALLENBACH, A., et al., Plasma Phys. Control. Fusion **33** (1991) 595.
[11] ASAKURA, N., et al., Nucl. Fusion **33** (1993) 1165.
[12] BELL, M.G., Nucl. Fusion **19** (1979) 33.
[13] YAMAMOTO, S., et al., in Plasma Physics and Controlled Nuclear Fusion Research 1982 (Proc. 9th Int. Conf. Baltimore, 1982), Vol. 1, IAEA, Vienna (1983) 73.
[14] ISLER, R.C., et al., Appl. Phys. Lett. **42** (1983) 355.
[15] KOSTEK, C.A., et al., Plasma Phys. **25** (1983) 421.
[16] BRAU, K., et al., Nucl. Fusion **23** (1983) 1643.
[17] BUGARYA, V.I., et al., Nucl. Fusion **25** (1985) 1707.
[18] HAWKES, N.C., PEACOCK, N.J., Nucl. Fusion **25** (1985) 971.
[19] BITTER, M., et al., Phys. Rev. A **32** (1985) 3011.
[20] ISLER, R.C., et al., Nucl. Fusion **26** (1986) 391.
[21] MATTIOLI, M., et al., J. Appl. Phys. **64** (1988) 3345.
[22] BARTIROMO, R., et al., Rev. Sci. Instrum. **60** (1989) 237.
[23] WEISEN, H., et al., Nucl. Fusion **29** (1989) 2187.
[24] PEEBLES, W.A., et al., in Plasma Physics and Controlled Nuclear Fusion Research 1990 (Proc. 13th Int. Conf. Washington, DC, 1990), Vol. 1, IAEA, Vienna (1991) 589.
[25] SCOTT, S.D., et al., Phys. Rev. Lett. **64** (1990) 531.
[26] IDA, K., et al., Nucl. Fusion **31** (1991) 943.
[27] ERIKSSON, L.-G., et al., Plasma Phys. Control. Fusion **34** (1992) 863.
[28] DUVAL, B.P., JOYE, B., MARCHAL, B., Nucl. Fusion **32** (1992) 1405.
[29] KOIDE, Y., et al., in Plasma Physics and Controlled Nuclear Fusion Research 1992 (Proc. 14th Int. Conf. Würzburg, 1992), Vol. 1, IAEA, Vienna (1993) 777.
[30] NAGASHIMA, K., et al., Nucl. Fusion **34** (1994) 449.
[31] HSUAN, H., et al., AIP Conf. Proc. **355** (1996) 39.
[32] ERIKSSON, L.-G., et al., Plasma Phys. Control. Fusion **39** (1997) 27.
[33] RICE, J.E., et al., Nucl. Fusion **37** (1997) 421.
[34] KIM, Y.B., DIAMOND, P.H., GROEBNER, R.J., Phys. Fluids B **3** (1991) 2050.
[35] HUTCHINSON, I.H., et al., Phys. Plasmas **1** (1994) 1511.
[36] GOLOVATO, S.N., et al., AIP Conf. Proc. **355** (1996) 23.
[37] KÄLLNE, E., KÄLLNE, J., MARMAR, E.S., RICE, J.E., Phys. Scr. **31** (1985) 551.
[38] RICE, J.E., et al., Rev. Sci. Instrum. **61** (1990) 2753.
[39] ERICKSON, G.W., J. Phys. Chem. Ref. Data **6** (1977) 831.
[40] MARMAR, E.S., et al., Phys. Rev. A **33** (1986) 774.
[41] VAINSHTEIN, L.A., SAFRONOVA, U.I., Phys. Scr. **31** (1985) 519.
[42] RICE, J.E., et al., Phys. Rev. A **35** (1987) 3033.

[43] RICE, J.E., et al., Rev. Sci. Instrum. **66** (1995) 752.
[44] GREENWALD, M., et al., Nucl. Fusion **37** (1997) 793.
[45] TAKASE, Y., et al., in Fusion Energy 1997 (Proc. 16th Int. Conf. Montreal, 1996), Vol. 1, IAEA, Vienna (1997) 475.
[46] YUSHMANOV, P., et al., Nucl. Fusion **30** (1990) 1999.
[47] MIGLIUOLO, S., Nucl. Fusion **33** (1993) 1721.
[48] LAO, L.L., et al., Nucl. Fusion **25** (1985) 1611.
[49] HALLOCK, G.A., et al., Phys. Rev. Lett. **56** (1986) 1248.
[50] CONNOR, J.W., et al., Plasma Phys. Control. Fusion **29** (1987) 919.

(Manuscript received 4 April 1997
Final manuscript accepted 10 October 1997)

E-mail address of J.E. Rice:
rice@trilm.psfc.mit.edu

Subject classification: F1, Te; G2, Te